© 2018. Published by The Company of Biologists Ltd | Development (2018) 145, dev166363. doi:10.1242/dev.166363

STEM CELLS AND REGENERATION

RESEARCH ARTICLE

Diverse progenitor cells preserve salivary gland ductal architecture after radiation-induced damage

Alison J. May[1,2], Noel Cruz-Pacheco[1,2], Elaine Emmerson[1,2,*], Eliza A. Gaylord[1,2], Kerstin Seidel[1,3,‡], Sara Nathan[1,2], Marcus O. Muench[4], Ophir D. Klein[1,3,5] and Sarah M. Knox[1,2,§]

ABSTRACT

The ductal system of the salivary gland has long been postulated to be resistant to radiation-induced damage, a common side effect incurred by head and neck cancer patients receiving radiotherapy. Yet, whether the ducts are capable of regenerating after genotoxic injury, or whether damage to ductal cells induces lineage plasticity, as has been reported in other organ systems, remains unknown. Here, using the murine salivary gland, we show that two ductal progenitor populations, marked exclusively by KRT14 and KIT, maintain non-overlapping ductal compartments after radiation exposure but do so through distinct cellular mechanisms. KRT14$^+$ progenitor cells are fast-cycling cells that proliferate in response to radiation-induced damage in a sustained manner and divide asymmetrically to produce differentiated cells of the larger granulated ducts. Conversely, KIT$^+$ intercalated duct cells are long-lived progenitors for the intercalated ducts that undergo few cell divisions either during homeostasis or after gamma radiation, thus maintaining ductal architecture with slow rates of cell turnover. Together, these data illustrate the regenerative capacity of the salivary ducts and highlight the heterogeneity in the damage responses used by salivary progenitor cells to maintain tissue architecture.

KEY WORDS: Radiotherapy, Stem cells, Regeneration, Salivary gland, KRT14, KIT

INTRODUCTION

Salivary glands (SGs) are composed of a complex architecture of saliva-synthesizing acini and transporting ducts capable of producing up to 1.5 liters of sero-mucous liquid per day (in humans). The epithelium coordinating this secretory program is very heterogeneous in cell type and consists of two kinds of acinar cells (mucous and serous) and at least three kinds of ductal cells of increasing size [intercalated (smallest), granulated/striated and excretory (largest)]. These cells are morphologically and functionally distinct, allowing the organ to alter the composition of the saliva under unstimulated and stimulated conditions (e.g. food intake). Such cell diversity implies that maintenance of tissue during homeostasis or after injury occurs either via differentiation of multipotent progenitors capable of producing multiple lineages or through distinct progenitor populations that act to replace a single cell type. In support of the latter model, over the last few years a number of distinct progenitor cell populations have been identified to contribute to one of the multiple cell types constituting the adult epithelium. SOX2$^+$ cells replenish acinar cells of the adult sublingual gland (SLG) (Emmerson et al., 2018), and KRT14$^+$/KRT5$^+$ cells give rise to the granulated ductal lineage of the submandibular gland (Kwak et al., 2016; Weng et al., 2018). Recently, we identified KIT$^+$ cells as a second progenitor population for the ductal lineage that give rise to the intercalated ducts (IDs) of the adult SLG (Emmerson et al., 2018), further supporting the requirement for multiple progenitors in SG homeostasis. However, the mechanisms by which these progenitors replace ductal cells, whether they acquire lineage plasticity to replace multiple cell types and their ability to regenerate the ductal system after damage is unknown.

Salivary glands originate from an invagination of the oral epithelium into a condensing mesenchyme [embryonic day (E) 11.5, 6-8 weeks in humans] and form an initial pre-acinar 'end bud' on what will become the secretory duct for the oral cavity. This single pre-acinar end bud undergoes rapid expansion, cleft formation, duct formation, lumenization and terminal differentiation to form a highly branched lobular structure capable of producing saliva by birth (Tucker, 2007). The murine ductal lineage emerges from a relatively undifferentiated population of KRT5$^+$KRT19$^-$ progenitors that differentiate to form the morphologically and functionally distinct KRT8-enriched intercalated, MUC19$^+$ granulated/striated and KRT19$^+$ excretory ducts (Knox et al., 2010; Lombaert et al., 2013). These ducts differ vastly in size, with IDs connecting the acini to the ductal system being the smallest and excretory ducts residing in the connective tissue connecting the oral cavity to this system being the largest. Furthermore, the ductal cells themselves differ in size, shape and function: IDs are composed of small cuboidal cells that passively absorb ions from the saliva, whereas the large columnar cells of the striated ducts actively absorb Na^+ and secrete $HCO3^-$ (Lee et al., 2012).

Salivary glands are inadvertently injured from radiation treatment delivered to patients for the elimination of head and neck tumors [~60,000 new patients per year in USA (Siegel et al., 2015)]. Off-target radiation destroys saliva-synthesizing acinar cells (Redman, 2008; Sullivan et al., 2005) and results in a lifetime of dry mouth and associated co-morbidities, such as oral infections, poor wound healing and dental decay (Brown et al., 1975; Dreizen et al., 1977; Dusek et al., 1996). We recently showed that acinar progenitors can replenish the acini immediately after radiation-induced damage (Emmerson et al., 2018). Intriguingly, the ductal system seems far less perturbed after radiation treatment than the acini, with ducts marked by KRT5 being similar in phenotype to non-irradiated tissue (Knox et al., 2013). However, whether the ducts actively regenerate after radiation and whether this is mediated by one or more populations of progenitor cells is unknown.

[1]Program in Craniofacial Biology, University of California, 513 Parnassus Avenue, San Francisco, CA 94143, USA. [2]Department of Cell and Tissue Biology, University of California, 513 Parnassus Avenue, San Francisco, CA 94143, USA. [3]Department of Orofacial Sciences, University of California, 513 Parnassus Avenue, San Francisco, CA 94143, USA. [4]Blood Systems Research Institute, San Francisco, CA 94118, USA. [5]Department of Pediatrics and Institute for Human Genetics, University of California, San Francisco, San Francisco, CA 94143, USA.
*Present address: The MRC Centre for Regenerative Medicine, The University of Edinburgh, Edinburgh, UK. ‡Present address: Department of Discovery Oncology, Genentech, South San Francisco, CA 94080, USA.

§Author for correspondence (sarah.knox@ucsf.edu)

S.N., 0000-0002-0090-0303; S.M.K., 0000-0002-6286-9997

Received 5 April 2018; Accepted 2 October 2018

Development (2018) 145, dev166363. doi:10.1242/dev.166363

Here, we show that the submandibular salivary ductal network is maintained during homeostasis and after genotoxic injury by KRT14$^+$ and KIT$^+$ progenitors that differ dramatically in their regenerative behavior. Using short- and long-term lineage tracing, we demonstrate that KRT14$^+$ and KIT$^+$ cells are unique, non-overlapping progenitor populations for the ductal lineage that replenish specific cellular compartments during homeostasis and after damage. We also demonstrate that these cells do not acquire lineage plasticity after radiation-induced damage, thereby limiting repair of each ductal cell type solely to its single progenitor. Finally, we show that KRT14$^+$ and KIT$^+$ populations differ substantially in how they preserve tissue architecture in the face of genotoxic injury, with KRT14$^+$ cells repopulating ductal cells primarily through asymmetric division, whereas KIT$^+$ cells maintain ductal tissue structure through limited cell turnover.

RESULTS

KRT14 and KIT segregate during development to mark distinct ductal cells in both mice and humans

Although both KIT$^+$ and KRT14$^+$ cells have been demonstrated to give rise to ducts in the adult salivary gland (Emmerson et al., 2018; Kwak et al., 2016), whether KIT and KRT14 mark the same ductal progenitor cell in the submandibular gland (SMG) and whether KIT$^+$ cells give rise to acinar cells during development, similar to the KRT14$^+$ cells, remains unclear. We first determined the location of KIT and KRT14 protein in adult murine SMG. KRT14 was expressed by smooth muscle actin-positive (SMA$^+$) myoepithelial cells as well as by a group of four to eight KRT5$^+$ SMA$^-$ cells located at the acinar-ID and ID-granulated duct (GD) junctions (Fig. 1A and Fig. S1A). Although located distal to the granulated duct, KRT14$^+$ SMA$^-$ cells did not express the granulated duct cell

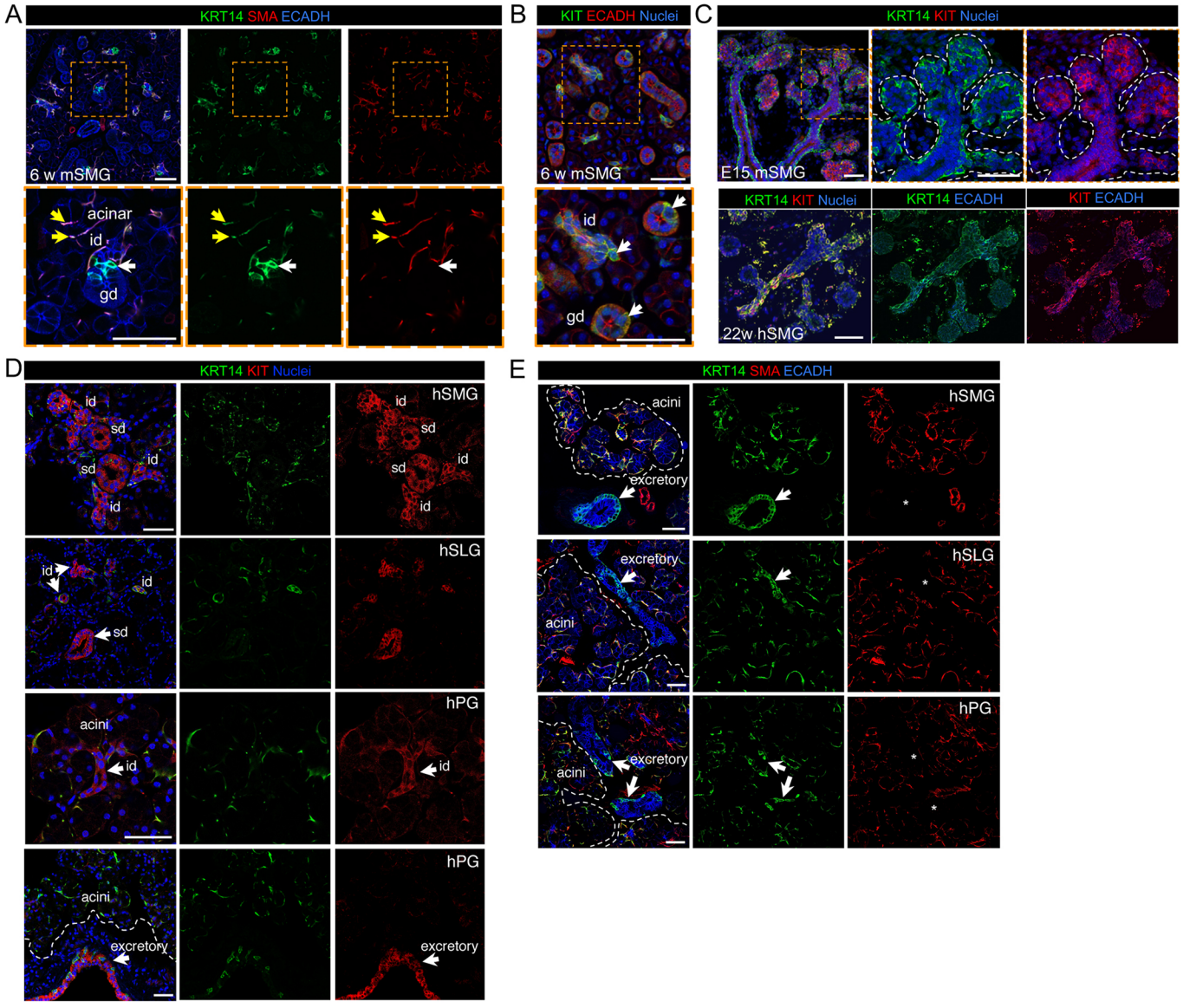

Fig. 1. KRT14 and KIT mark distinct populations of ductal cells in murine and human SG. (A-E) Murine (m) adult (A,B, *n*=3) and embryonic day 15 (E15, C, *n*=3) submandibular gland (SMG) or human (h) fetal (C, *n*=1) and adult (D,E, *n*=1) SMG, sublingual gland (SLG) and parotid gland (PG) immunostained for KIT, KRT14, SMA and E-cadherin. Scale bars: 50 µm. id, intercalated duct; gd, granulated duct; sd, striated duct. White arrows in A indicate KRT14$^+$ SMA$^-$ ductal cells; yellow arrows in A indicate KRT14$^+$ SMA$^+$ myoepithelial cells; arrows in B indicate KIT expression in id and gd; arrows in E indicate KRT14$^+$ SMA$^-$ ductal cells, Asterisks in E indicate absence of SMA staining in ductal cells. White perforated line outlines SG epithelium (C) or acini (D,E). *n*=number of animals or human subjects.

Development (2018) 145, dev166363. doi:10.1242/dev.166363

marker MUC19 (Fig. S1B). As previously reported in the SLG (Emmerson et al., 2018), KIT expression was observed predominantly in the SMG IDs, as well as granulated duct cells, albeit at a substantially lower level of expression (Fig. 1B). This restricted expression of KRT14 and KIT to the ductal and/or myoepithelial lineages contrasts to developing E13-E14 SMG, where both acinar and duct cells express KRT14 and KIT (Lombaert et al., 2013). However, segregation of these proteins in the acinar cells begins before terminal differentiation (~E15), with few KRT14$^+$ cells expressing KIT (Fig. 1C), suggesting embryonic segregation of these lineages has already occurred at this stage.

Despite KIT being a well-studied receptor in stem cell biology that has been postulated to be involved in the regeneration of salivary glands (Nanduri et al., 2013), the localization of KIT in developing or adult human SG is unclear. The development of human SG is similar to the mouse (Teshima et al., 2016) with the formation of a branched undifferentiated epithelium from the buccal mucosa that undergoes terminal differentiation and maturation to produce a functional acinar-ductal network by birth. Similar to the early embryonic murine SMG, we found that in the human SMG, KIT and KRT14 are co-expressed in both acinar and ductal cells during fetal development (22 weeks, Fig. 1C), suggesting that at 22 weeks the human organ was reflective of <E15 murine SMG (the precise timing of human SG differentiation and maturation is not known). However, in the adult human SMG, KIT and KRT14 no longer colocalized, with KIT enriched in intercalated as well as larger striated ductal cells, while KRT14 was highly expressed by basal cells of the excretory ducts and SMA$^+$ myoepithelial cells (Fig. 1D-E). As for murine SMG, we also observed KRT14$^+$ cells that were either SMA$^+$ or SMA$^-$ (Fig. 1A), indicating myoepithelial and basal duct cells, respectively. Similar expression patterns were also observed for KRT14 and KIT in the adult human SLG and parotid gland (PG) (Fig. 1D,E). Thus, the adult mouse SMG recapitulates the adult human gland, confirming it as a useful system for modeling these divergent cell types.

KRT14 and KIT expression is dynamically expressed during postnatal remodeling of the ductal compartment

During all stages of postnatal murine SMG development (P2-P30), SMA$^+$ myoepithelial cells retained expression of KRT14 (Fig. 2A). However, SMA-negative ductal cells showed dynamic changes in KRT14 expression during maturation of the ductal system (P2-P30), a period that includes establishment of the granulated ducts (GD) [at around postnatal day (P) 14 (Harvey, 1952; Gresik, 1994)]. At P2, we found KRT14 to be expressed by basal duct cells that constitute 46±2% of the total ductal population (Fig. 2A,B). These SMA-negative cells were also proliferative, with 17±2.5% incorporating EdU (Fig. 2A,C; EdU injected 2 h before animal sacrifice). From P7, we observed apical expression of KRT14 in initiating GD cells (Fig. 2A, yellow outlines, G) bringing the total percentage of KRT14$^+$ cells in the ductal compartment to 73±6.6% by P14 (Fig. 1A-C). However, by P30 most GD cells no longer expressed KRT14, and junctional KRT14$^+$ SMA$^-$ cells were becoming restricted to the acini-ID and ID-GD junctions (Fig. 2A, white arrows, G). These junctional ductal cells represented 39±5% of total ductal cells, and were proliferating at a similar rate to KRT14$^+$SMA$^-$ cells of the P14 SMG (5±0.3% KRT14$^+$ SMA$^-$ EdU$^+$; Fig. 2A-C), suggesting that they maintain a progenitor cell-like state.

As KRT5 is also a marker of basal epithelial cells in multiple organs, including the duct cells of the adult salivary gland (Rock et al., 2009; Van Keymeulen et al., 2011; Weng et al., 2018), we quantified the number of cells expressing KRT5 and KRT14 during embryonic and postnatal development. Although KRT5 was always expressed in KRT14$^+$ cells (Fig. S1, Table S2), we unexpectedly found a subset of KRT14$^+$ cells that did not express KRT5. As shown in Fig. S1C,D, KRT5 labeled a subset of KRT14$^+$ basal cells lining ducts from P2 to P30 but unlike KRT14, KRT5 is not expressed by myoepithelial cells at P2 and P7 (Fig. S1D), suggesting KRT14 and not KRT5 is an early marker of the myoepithelial cell lineage.

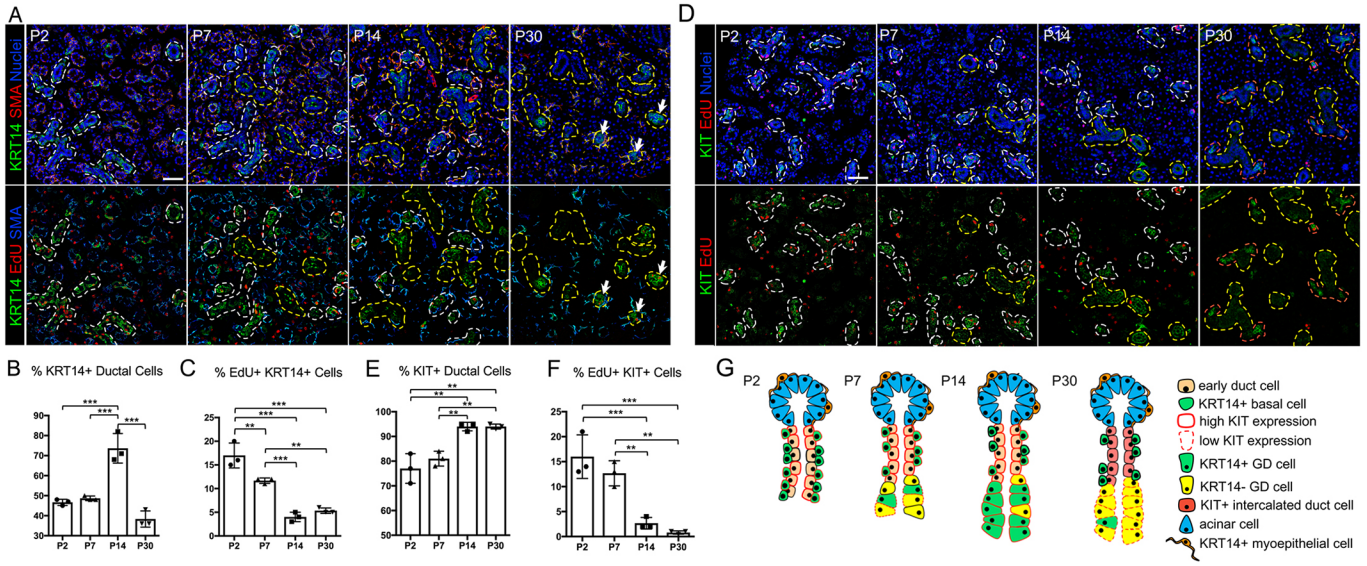

Fig. 2. KRT14 and KIT have dynamic expression during postnatal murine SMG development. (A) Expression and proliferation analysis of KRT14$^+$ SMA$^-$ ductal cells during postnatal SMG development. (B,C) Number of and proliferation of KRT14$^+$ SMA$^-$ cells were quantified. (D) Expression and proliferation analysis of KIT$^+$ ductal cells during postnatal SMG development. (E,F) Number of and proliferation of KIT$^+$ cells was quantified. (G) Schematic representation of KRT14 and KIT expression during postnatal SMG ductal development. Scale bars: 50 µm. (A,D) Early ducts are outlined in white; granulated ducts outlined in yellow; mature KIT$^+$ intercalated duct cells are outlined in red; restricted locations of KRT14$^+$ SMA$^-$ basal cells are indicated by white arrows. *n*=3 for all ages, where *n* indicates number of animals. Sex was randomized for P2, P7 and P14; female mice were analyzed at P30. **P*<0.05, ***P*<0.01, ****P*<0.001, one-way analysis of variance, Tukey's multiple comparison. Data are mean±s.d.

Development (2018) 145, dev166363. doi:10.1242/dev.166363

Although KIT is predominantly found in pre-acinar end buds before terminal differentiation (E16) (Lombaert et al., 2013), by P2 KIT was no longer expressed by acinar cells and became localized to early luminal and KRT14$^+$ basal ductal cells (Fig. 2D,E; 77±6% total ductal cells). Similar to KRT14$^+$ cell dynamics, the number of KIT$^+$ ductal cells increased significantly from P7 to P14 (81±3% to 94±2% of total ductal cells) with the appearance of KIT-expressing cells throughout the developing GD, albeit at lower levels compared with that in the ID cells (Fig. 2D,G). By P30, the majority of ID and GD cells were KIT$^+$ (94±1% of all ductal cells); however, KIT and KRT14 were no longer co-expressed by intercalated or GD cells (Fig. 2A,D,G, Fig. S1C). This segregation of KRT14 and KIT protein in the ductal system was accompanied by a dramatic reduction in the proliferation rate of KIT$^+$ cells from 16% at P2 to 1±0.3% by P30 (compared with 12% at P2 to 4% at P30 for KRT14$^+$ cells), suggesting that the KIT$^+$ IDs and GDs have limited ability to repopulate the ducts by the early adult stage.

KRT14$^+$ and KIT$^+$ cells are multipotent progenitors during SG development that become unipotent to produce a single non-overlapping ductal cell type

As KIT and KRT14 colocalize during development (Lombaert et al., 2013) and KRT14 is expressed by the oral epithelium before ontogenesis (Emmerson et al., 2017), we first asked whether KRT14$^+$ cells give rise to KIT$^+$ cells by performing inducible genetic lineage tracing using *Krt14*^{CreERT2} crossed to a *Rosa26*^{mTmG} reporter line. Similar to a previous study using a non-inducible *Krt14* promoter (Lombaert et al., 2013), we found that Cre activation at E10.5 (before invagination) and E12.5 resulted in GFP$^+$ cells marking the entire E16.5 epithelial compartment (including acinar, duct and myoepithelial cells; Fig. 3A) and confirmed that KRT14$^+$ progenitor cells give rise to KIT$^+$ cells (Fig. 3A). However, when lineage tracing was initiated at P2 [before the emergence of GD (Srinivasan and Chang, 1979)] and P30 (when the ductal system is fully differentiated), KRT14$^+$ cells contributed solely to the ductal compartment and, more specifically, to granulated ducts (Fig. 3B,C), indicating that the fate of KRT14$^+$ cells is determined at or before P2.

Next, we tested whether KIT$^+$ cells also became lineage restricted by P2 by using an inducible Cre driven by the *Kit* promoter (*Kit*^{CreERT2}). In contrast to KRT14$^+$ cells, activation of Cre at P2 resulted in both GFP$^+$ acinar and duct cells (but not myoepithelial cells), indicating that KIT$^+$ progenitors maintained their multipotency for longer (Fig. 4A). However, by 6 weeks of age, KIT$^+$ cells replenished the IDs (KRT8$^+$ KIT$^+$) but not acinar cells (AQP5$^+$) or KRT14$^+$ cells surrounding these ducts (Fig. 4B-D). Although we did find endogenous KIT expression in GD cells (Fig. 4B), some of which were labeled at 24 h and 14 days after Cre activation (Fig. 4B, Fig. S1F), few GFP$^+$ cells per GD were found later in tissue traced for 6 months (Fig. 4D), indicating that KIT$^+$ GD cells do not repopulate this compartment. Together, these data indicate that both KIT$^+$ and KRT14$^+$ cells contribute to multiple epithelial lineages of the developing SMG and become lineage restricted at distinct time points to produce non-overlapping duct cell populations.

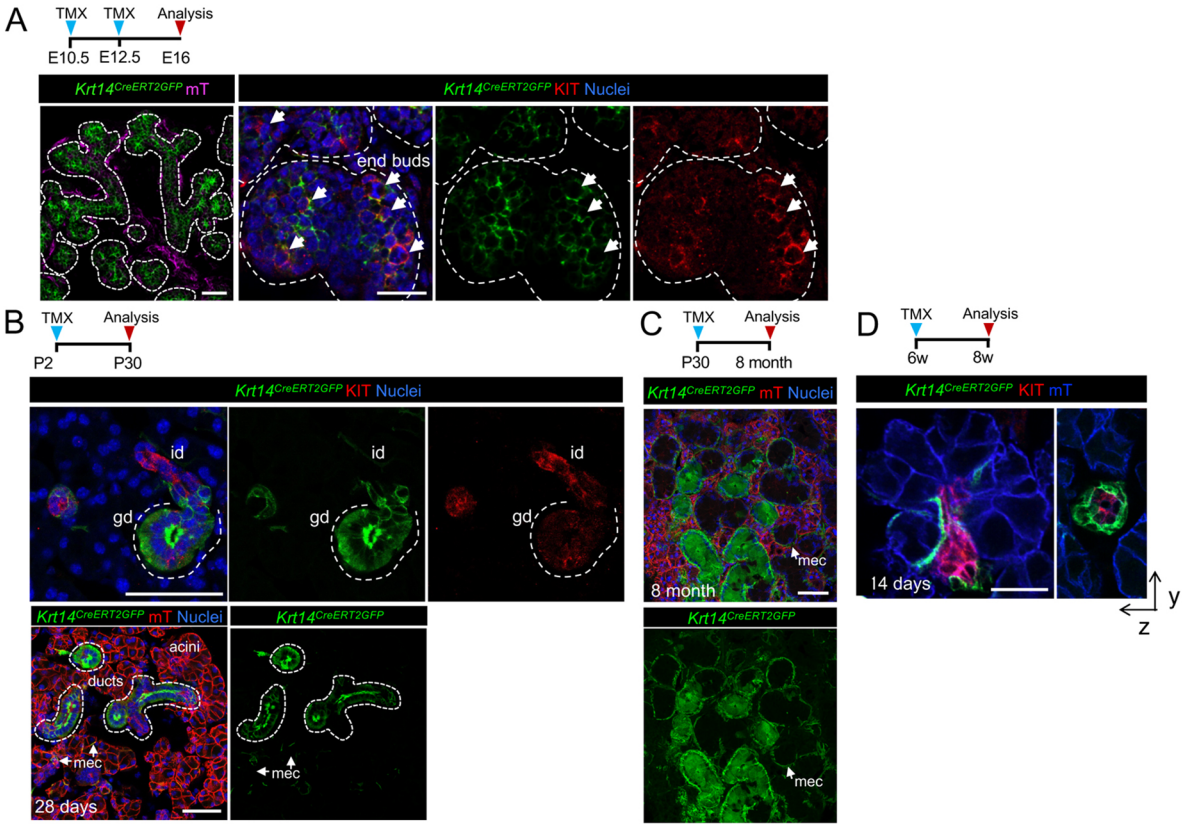

Fig. 3. KRT14$^+$ cells become lineage restricted to produce granulated ducts and not KIT$^+$ intercalated ducts. KRT14 expression and proliferation analysis of KRT14$^+$ SMA$^-$ ductal cells during postnatal SMG development. Genetic lineage tracing in *Krt14*^{CreERT2};*Rosa26*^{mTmG} was activated at E10.5 and E12.5 (A), P2 (B), P30 (D) or 6 weeks (D) and cells traced for 4 days to 8 months (as indicated), before being stained for KIT. Scale bars: 50 µm. Arrows in A indicate *Krt14*$^{CreERT2GFP+}$ KIT$^+$ end-bud cells; white outlines SG epithelium in A and granulated ducts in B. id, intercalated ducts, gd, granulated ducts; mec, myoepithelial cell.

Development (2018) 145, dev166363. doi:10.1242/dev.166363

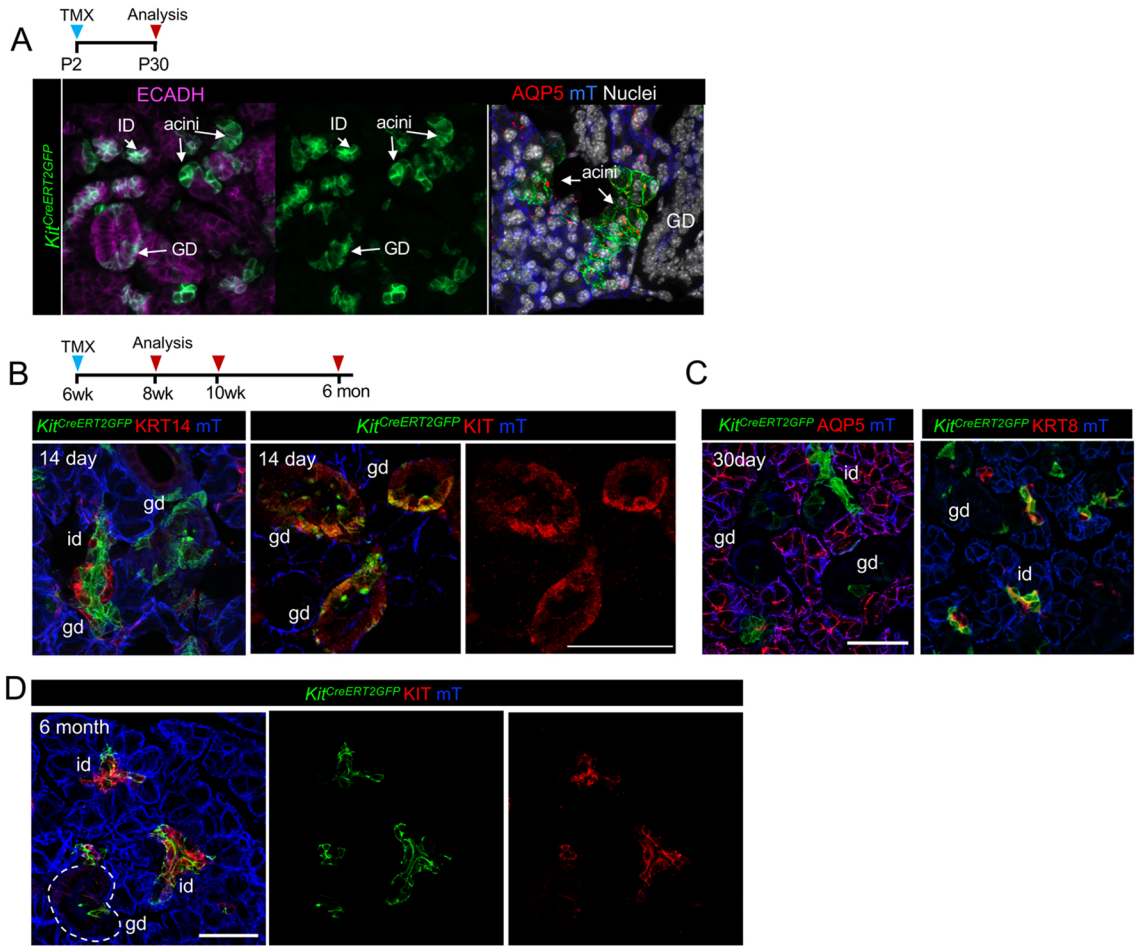

Fig. 4. KIT⁺ cells in the adult murine SMG contribute to the intercalated ducts but not KRT14⁺ cells. (A-D) Genetic lineage tracing in *Kit14*^{CreERT2};*Rosa26*^{mTmG} was activated at P2 (A) or 6 weeks (B-D) and cells traced for 14 or 30 days or 6 months (as indicated) before immunostaining for KRT14, KIT, the acinar marker AQP5 and the duct marker KRT8, and staining the nuclei. Scale bars: 50 µm. id/ID, intercalated duct; gd/GD, granulated ducts. P2-P20, *n*=2; 6-8 weeks, *n*=4; 6-10 weeks, *n*=2; 6 weeks-6 months, *n*=3. *n*=number of animals.

KRT14⁺SMA⁺ cells give rise to myoepithelial cells and not ductal or acinar cells

As KRT14$^+$ cells also contributed to the myoepithelial compartment (Fig. 3, Kwak et al., 2016), we next determined whether KRT14$^+$SMA$^+$ cells were capable of producing acinar or ductal cells by performing lineage tracing in an inducible Cre under the control of the *Acta2* promoter [*SMA*^{CreERT2} (Wendling et al., 2009)] crossed to an RFP reporter. During embryonic development, basal KRT14$^+$ cells in the end bud begin to express SMA with the emergence of these cells from the acini by E16 (Fig. 5A). However, a population of KRT14$^+$ cells within the ducts remains SMA negative (Figs 2 and 5A). Activation of *SMA*^{CreERT2} at E15 resulted in the production of SMA$^+$ myoepithelial cells, but not KRT14$^+$ ductal cells or AQP5$^+$ acinar cells (Fig. 5B), suggesting that lineage restriction for the myoepithelial cell lineage occurs at a time point preceding myoepithelial emergence from the basal epithelium of the end bud. This is in contrast to the acinar lineage, which we found to be derived from KRT14$^+$ cells up until E15 (Fig. 5C), with recombination at E16 resulting in the production of ductal and KRT14$^+$ SMA$^+$ myoepithelial cells only (Fig. S2). To determine whether SMA$^+$ cells contributed to other epithelial lineages in adult SMG, we activated *SMA*^{CreERT2} in 6-week-old adult mice and traced cells for 30 days and 6 months but found no contribution of SMA$^+$ cells to the ductal or acinar lineages (Fig. 5D,E), indicating that KRT14$^+$ myoepithelial cells give rise to themselves exclusively.

KRT14⁺ but not KIT⁺ cells replenish the ductal compartment after radiation-induced damage through asymmetric division

Radiotherapy for head and neck cancer leads to injury of the SG and causes an eventual loss of the acinar cell compartment (Knox et al., 2013; Grundmann et al., 2010). In contrast, the ductal compartment remains relatively intact after radiotherapy, suggesting that the ductal system has long-term regenerative or cell maintenance capacity (Knox et al., 2013). To determine whether ducts are capable of actively regenerating in response to genotoxic injury, we analyzed cell division of KRT14$^+$ SMA$^-$, KIT$^+$ and GD cells after a 10 Gy dose of radiation was applied to the neck of wild-type C57BL6 mice and compared with uninjured (0 Gy) tissue. Similar to previous studies in the mouse and rat, we detected very limited proliferation (quantified as EdU uptake after a 2 h pulse) in the ductal system of the homeostatic gland (Kimoto et al., 2007; Chibly et al., 2014; Kim et al., 2008), with cell division being restricted almost exclusively to KRT14$^+$ SMA$^-$ junctional cells (3±1% KRT14$^+$ SMA$^-$ EdU$^+$ cells compared with 0.75±0.78% KIT$^+$ EdU$^+$ and 0.07±0.12% GD EdU$^+$ cells, Fig. 6A-F). After radiation-induced damage, the number of KRT14$^+$EdU$^+$ cells was initially reduced by 3 days post-irradiation (1±2%), suggestive of cell cycle exit. However, cell division increased significantly over time with 7±5% and 15±4% of KRT14$^+$ cells being EdU$^+$ at 7 and 14 days post-irradiation, respectively (Fig. 6A,B), indicating that these cells undergo delayed mitosis in response to irradiation-induced injury.

Development (2018) 145, dev166363. doi:10.1242/dev.166363

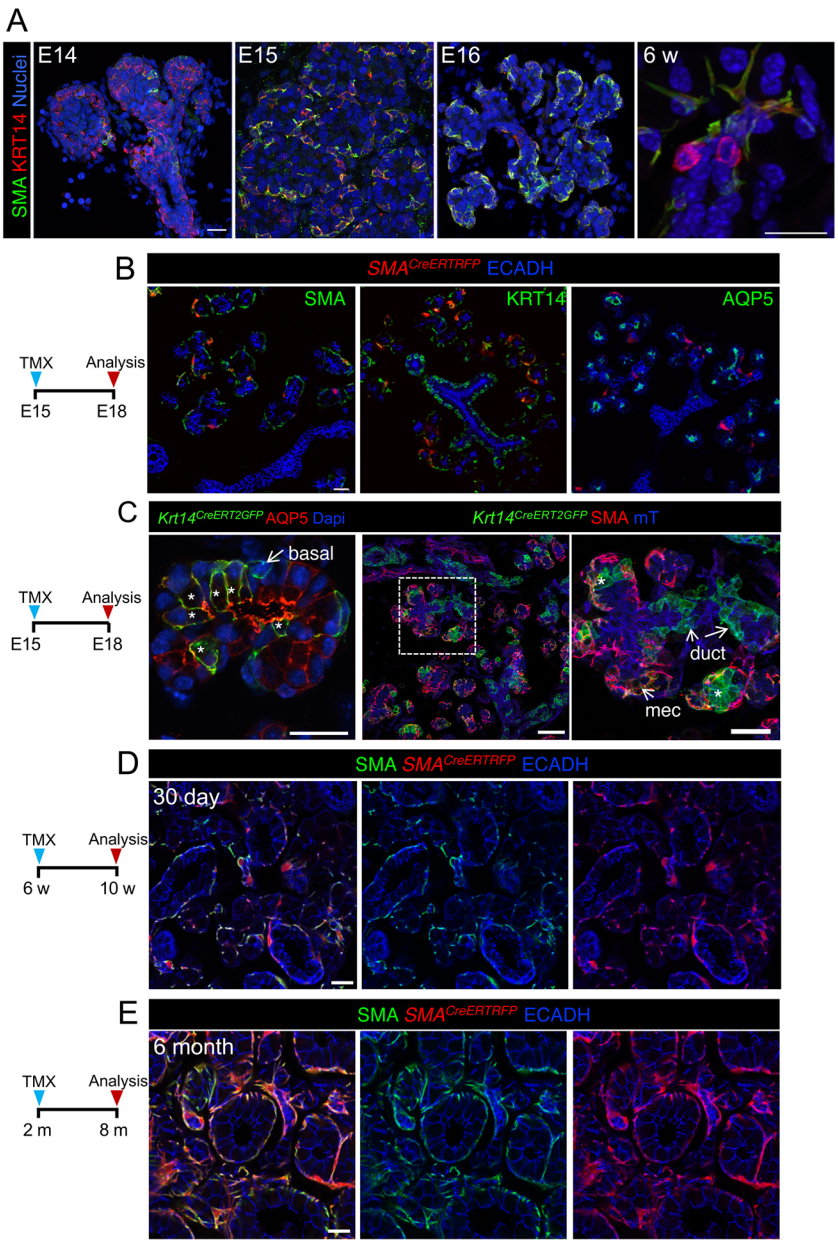

Fig. 5. KRT14$^+$ SMA$^+$ cells give rise to myoepithelial cells but not to duct or acinar cells. (A) KRT14 and SMA localization in developing (E14-E16) and adult (6 weeks) SMG. (B,C) Genetic lineage tracing was activated in *SMA^{CreERT};Rosa26^{mTmG}* (*n*=3) and *Krt14^{CreERT2};Rosa26^{mTmG}* at E15 (*n*=3). (D,E) Genetic lineage tracing was activated in *SMA^{CreERT};Rosa26^{mTmG}* mice at 6 weeks and traced for 30 days (*n*=1) and 6 months (*n*=1) before immunostaining for SMA (*n*=1). Scale bars: 20 µm. mec, myoepithelial cell. Asterisks indicate GFP$^+$ acinar cells. *n*=number of animals.

Similarly, the number of KRT14$^+$ SMA$^-$ cells located at each intercalated-granulated duct junction significantly decreased by 3 days post-irradiation, but recovered to homeostatic levels by 7 days post-irradiation (3.7±0.4 at day 7 and 4±1 at day 14; Fig. 6C). In contrast to KRT14$^+$ cells, we found no EdU$^+$ KIT$^+$ ID cells or EdU$^+$ GD cells under injury conditions on day 3 and day 7 (Fig. 6D-F, Table S6). Furthermore, analysis of KIT$^+$ and GD cells at 14 days post-irradiation revealed almost no increase in cell division when compared with non-irradiated SMG (1.12±0.23% KIT$^+$ EdU$^+$, 0.05±0.09% GD EdU$^+$, Fig. 6D-F), suggesting radiation exposure does not promote cell division in these cells. To determine whether KIT$^+$ or GD cells were capable of proliferating after radiation-induced damage, we administered EdU daily from day 7 to 14 days post-irradiation and quantified the number of KIT$^+$, GD$^+$ and KRT14$^+$ cells that incorporated EdU (Fig. 6G). As for the single EdU dose at 14 days post-irradiation, proliferation of KRT14$^+$ cells significantly increased in irradiated tissue after multiple EdU doses compared with non-irradiated control (KRT14$^+$ SMA$^-$ EdU$^+$ cells were 34±4% and 50±3% EdU$^+$ in non-irradiated and irradiated SMG, respectively; Fig. 6G,H). Although the number of EdU$^+$ KIT$^+$ and GD EdU$^+$ cells increased from <1.5% in single 2 h-chase EdU-injected mice to 5±1% and 2±1%, respectively, after seven doses, there was no significant increase in the number of dividing KIT$^+$ cells (8±2%) or GD cells (1±0.2%) 14 days after irradiation (Fig. 6G,H), indicating that KIT$^+$ and GD cells, unlike KRT14$^+$ cells, do not actively contribute to the injured ductal system via a proliferative mechanism.

Finally, we tested whether KRT14$^+$ and KIT$^+$ cells were capable of repopulating the ductal network after radiation-induced damage by performing genetic lineage tracing in irradiated or homeostatic SG using the *Krt14^{CreERT2}* and *Kit^{CreERT2}* promoters crossed to the reporter *Rosa26^{mTmG}*. Analysis of GFP$^+$ cells 24 h following tamoxifen administration confirmed that *Krt14^{CreERT};Rosa26^{mTmG}* and *Kit^{CreERT2};Rosa26^{mTmG}* animals have a 29±2% and 50±7% labeling efficiency of KRT14$^+$ junctional cells and KIT$^+$ ID cells, respectively (Fig. S1F,G). We found a 10 Gy dose of radiation

Development (2018) 145, dev166363. doi:10.1242/dev.166363

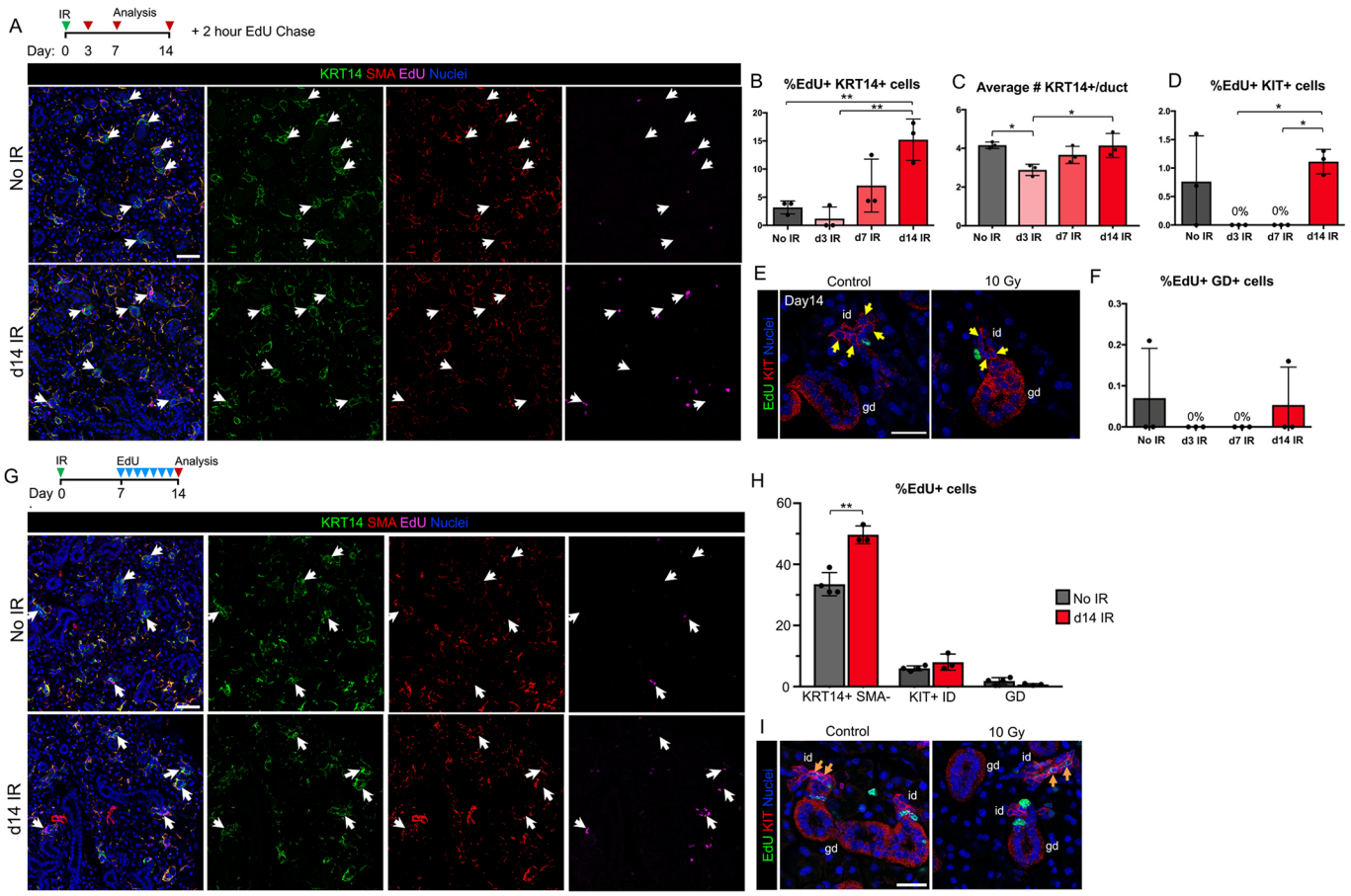

Fig. 6. KRT14$^+$ cells but not KIT$^+$ cells proliferate after radiation and replenish the ductal compartment through asymmetric division. (A,B,D,F) Adult female C57BL/6 mice were treated with 0 Gy (control, *n*=3) or 10 Gy (IR, *n*=3) and sacrificed 3, 7 or 14 days later with EdU being injected 2 h before collection. Number of proliferating cells (A) was then quantified (B,D,E,F). (C) Number of KRT14$^+$ SMA$^-$ progenitor cells located at each intercalated-granulated duct junction were quantified in control (No IR) and 3, 7 and 14 days post-IR mice. (D,E) Very little proliferation was found in KIT$^+$ intercalated duct (ID) cells (yellow arrows) at control or day 14 irradiated SGs, with no proliferation occurring at day 3 and day 7 post-irradiation. (F) Low rates of proliferation were found in granulated duct (GD) cells in control or day 14 irradiated SG, with no proliferation observed at day 3 and day 7 post-irradiation. (G-I) Adult female C57BL/6 mice were treated with 0 Gy (control, *n*=4) or 10 Gy (irradiated, *n*=3) and sacrificed 14 days later with EdU being injected daily for 7 days before collection. The number of proliferating cells was quantified in KRT14$^+$ SMA$^-$ progenitor cells (G,H), KIT$^+$ ID cells (H,I) and GD cells (H,I). White arrows in A and G indicate KRT14$^+$ SMA$^-$ progenitor cells; yellow arrows in E indicate EdU$^-$ KIT$^+$ ID cells in day 14 control and IR tissue. Scale bars: 50 µm in A,G; 25 µm in E,I. *P<0.05, **P<0.01, one-way analysis of variance, Tukey's multiple comparison (B-F), *t*-test (unpaired, two-tailed) (H). Data points in all graphs represent the count of each animal. *n*=number of animals. Data are mean±s.d.

resulted in extensive production of GFP$^+$ clones in the GD but no other ductal or acinar cell type in *Krt14^{CreERT2};Rosa26^{mTmG}* mice (Fig. 7A,B). Although endogenous KRT14 protein expression is absent from the granulated ducts (GD) after P30 and in adult glands, the *Krt14CreERT2* allele used in these experiments ectopically labels 23±10% of GD cells 24 h post-induction (Fig. S1G). As our analyses indicate that GD cells show almost no proliferation (0.05±0.09% GD EdU$^+$, Fig. 6F, day 14 post-irradiation) when compared with KRT14$^+$ SMA$^+$ cells (15±4% KRT14$^+$ SMA$^-$; Fig. 6B, day 14 post-irradiation), and we find a substantial increase in the number of GFP$^+$ clones within the GD after irradiation (Fig. 7A,B), we conclude that KRT14$^+$ cells but not GD cells actively replenish the GD. This conclusion is further supported by the recent findings that KRT14$^+$ cells give rise to GD cells during homeostatic conditions (Kwak et al., 2016), and KRT5$^+$ cells give rise exclusively to GD cells 30 days after irradiation (Weng et al., 2018). The specific repopulation of the GD cells by KRT14$^+$ basal cells is further supported by lineage tracing in irradiated *Kit^{CreERT2};Rosa26^{mTmG}* SG (Fig. 7C). Although some KIT-expressing GD cells were labeled 24 h (Fig. S1F) and 14 days after Cre induction (Fig. 4B) few GD cells were apparent 30 days after irradiation, whereas the IDs remained robustly GFP$^+$ (Fig. 7C), indicating that KIT$^+$ cells slowly repopulate themselves, but not other compartments (Fig. 8). As we routinely observed KIT$^+$ EdU$^+$ cells adjacent to each other (Fig. 6I), it is likely that these cells replenish their compartment by symmetrical division. As there was no increase in the number of KRT14$^+$ junctional duct cells on day 14 after injury (Fig. 6C), despite an increase in the percentage of KRT14$^+$ EdU+ cells dividing after irradiation (Fig. 6B), we conclude that KRT14$^+$ cells likely replenish themselves and the GD via asymmetric division (Fig. 8). Thus, KRT14$^+$ and KIT$^+$ cells represent distinct progenitor cells that use highly divergent cellular mechanisms to maintain ductal architecture after injury.

DISCUSSION

A large number of studies over the past 70 years have suggested that the ductal system is comparatively more resistant to radiation-induced damage than the acinar cells (Redman, 2008; Grundmann et al., 2010). Yet this observation had not been empirically studied. Our recent finding that acinar cells are capable of regenerating immediately after radiation exposure (Emmerson et al., 2018) strongly suggested that the ductal system could also regenerate in

Development (2018) 145, dev166363. doi:10.1242/dev.166363

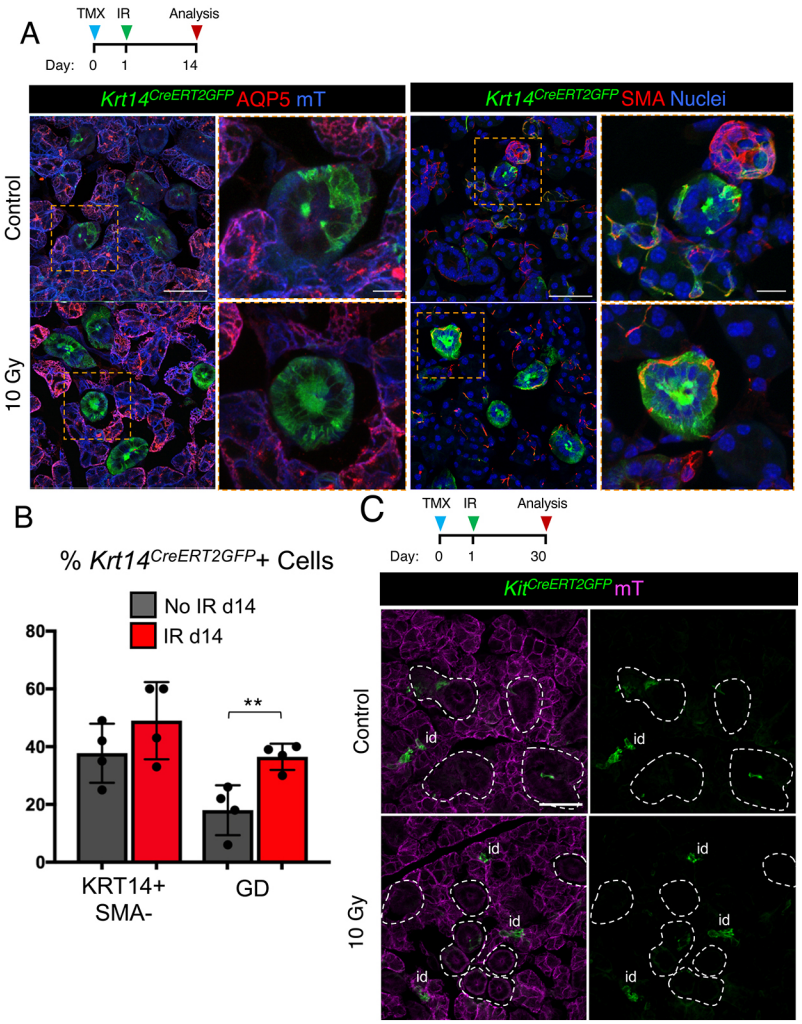

Fig. 7. KRT14$^+$ and KIT$^+$ cells maintain the ductal compartment after radiation-induced damage. (A-C) Lineage tracing was performed in *Krt14^{CreERT2};Rosa26^{mTmG}* (A,B) or *Kit^{CreERT2};Rosa26^{mTmG}* (C) female mice at 6-8 weeks with Cre activation 24 h before treatment with 0 or 10 Gy of gamma radiation. SG were then traced for 14 or 30 days. (B) *Krt14^{CreERT2GFP}* lineage tracing was quantified in KRT14$^+$ SMA$^-$ ductal progenitor cells and granulated duct (GD) cells. $^{**}P<0.01$, *t*-test (unpaired, two-tailed). In A, orange boxed area in left panel indicates position of magnified image in right panel. White lines in C outline GDs. ID, intercalated duct. *Krt14^{CreERT};Rosa26^{mTmG}* control, *n*=4; irradiated, *n*=4; *Kit^{CreERT2};Rosa26^{mTmG}* control, *n*=2 female; irradiated, *n*=2 female. *n*=number of animals. Data are mean±s.d. Scale bars: 50 µm in A,C; 20 µm in magnified panels in A.

response to genotoxic injury. Consistent with this prediction, we show that ducts can indeed regenerate after radiation-induced damage; however, cell replacement primarily occurs in the granulated ducts and is mediated by KRT14$^+$ cells. In contrast, KIT$^+$ cells show little turnover to maintain themselves, possibly surviving through increased resistance to DNA damage-mediated cell death to ensure tissue architecture remains unperturbed. Furthermore, we also find that these progenitors, like the SOX2$^+$ acinar progenitors, do not gain lineage plasticity in response to radiation, thereby ruling out a regenerative mechanism used by other organs such as the skin (Page et al., 2013; Ito et al., 2005) to ensure organ fidelity. Thus, these data indicate that the salivary ductal progenitor cells possess regenerative capacity but that there is heterogeneity in the mechanisms by which they maintain the organ.

Epithelial stem cells can divide by symmetric or asymmetric division, which allows for the expansion of their numbers and the production of differentiated cells (Itzkovitz et al., 2012; El-Hashash and Warburton, 2012; Lechler and Fuchs, 2005). An excellent example of this is a recent study of prostate basal and luminal cells: the basal cells exhibit both asymmetric and symmetric division to self-renew and produce differentiated luminal progeny, whereas the luminal cells divide by symmetric division to produce themselves (Wang et al., 2014). We have previously shown that basal cells in the lacrimal gland undergo asymmetric division to produce luminal daughter cells (Farmer et al., 2017) and our data in the SMG suggests a similar outcome for the basal KRT14$^+$ cells lining the excretory ducts. Intriguingly, as the KRT14$^+$ cells lie outside the granulated ducts (at the acini-ID and ID-GD junctions, Fig. 8), these daughter cells must incorporate into the larger ductal system and produce a cell vastly different in morphology from the original KRT14$^+$ cell. Indeed, such a mechanism was first predicted to occur in the rat SG by Man and co-workers, who defined a subset of junctional ID cells (but only rare GD cells) that incorporated radioactive thymidine (Man et al., 2001). Yet how this morphological transformation is achieved remains to be resolved. Similar to the luminal cell of the prostate, our lineage-tracing and proliferation studies suggest KIT$^+$ cells of the IDs undergo symmetric divisions, producing themselves over and over again albeit at a very slow rate. It is likely that symmetric division is slow in these cells due to the confined size of the IDs, which are typically only 10 cells in length. Their long-lived nature is also supported by previous label-retaining studies in adult rodents, showing that ID cells retain BrdU for more than 7 weeks after their initial labeling (Chibly et al., 2014). Although this outcome also suggests that KIT$^+$ cells are progenitors for the ID, we cannot rule out the possibility that they may be transit-amplifying cells derived from another as yet unknown progenitor cell source. Further investigation is necessary to understand why KIT$^+$ and KRT14$^+$ cells are restricted to

Development (2018) 145, dev166363. doi:10.1242/dev.166363

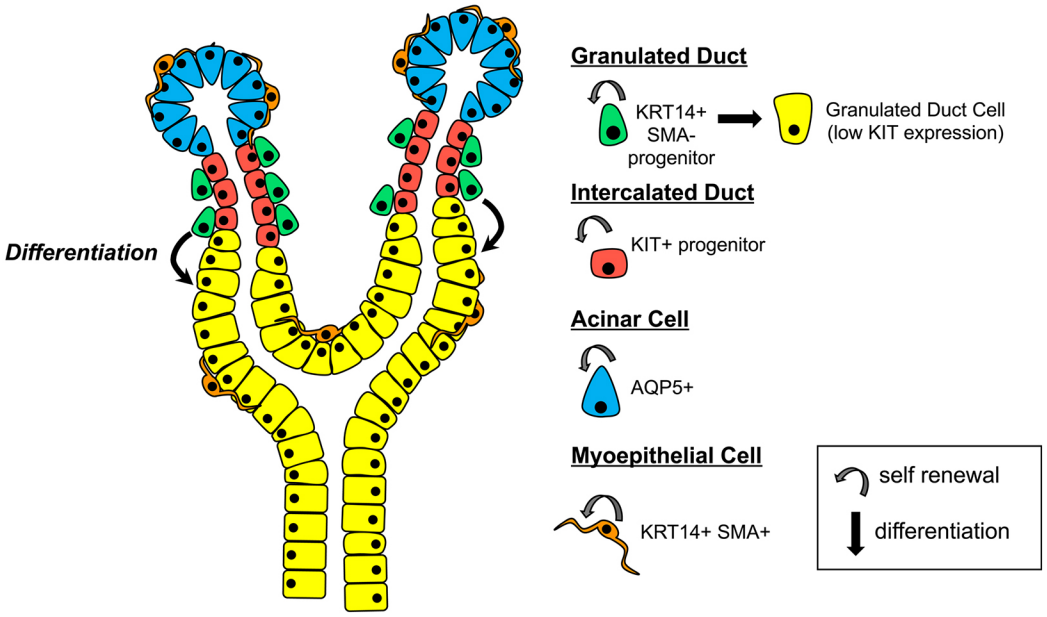

Fig. 8. Schematic representation of the heterogeneous progenitor populations that maintain and replenish the adult SG under homeostatic and injury conditions. KRT14$^+$ SMA$^-$ progenitor cells self-renew and give rise to differentiated KIT-positive granulated duct cells but do not contribute to the acinar or intercalated duct (ID) compartments. KIT$^+$ ID cells are long lived and slow dividing, and maintain the ID compartment. KRT14$^+$ SMA$^+$ myoepithelial cells (MECs) self-renew and maintain the MEC population. AQP5$^+$ acinar cells self-renew and replenish the acinar cell population.

symmetric and asymmetric divisions, as well as the mechanisms regulating the quiescence of KIT$^+$ cells.

We recently reported that murine acinar progenitor cells marked by SOX2 are highly regenerative, at least in the first 30 days after radiation exposure, and are capable of repopulating the acini similar to uninjured controls (Emmerson et al., 2018). Similarly, here we find that the ductal system can also replenish itself to some extent after genotoxic shock through KRT14$^+$ cells. KRT14$^+$ cell proliferation increases in the 2 weeks after radiation exposure, suggesting there is feedback from the granulated ducts to promote replenishment of these cells. However, whether this regenerative capacity can be sustained over the long term is unclear. Previous studies indicating that murine salivary glands degenerate/senesce 3-6 months after radiation suggest ducts may only regenerate for a limited time (Marmary et al., 2016; Muhvic-Urek et al., 2006). As these investigations focused on the acini rather than ducts, it remains to be determined whether the regenerative capacity of KRT14$^+$ cells does fail eventually and further analysis is required to discern the cause. It also remains to be determined whether the human salivary gland ductal system actively regenerates in the days/months after therapeutic radiation and whether this regenerative capacity fails in the long term due to the inability of progenitors to enter the cell cycle.

How these KRT14$^+$ and KIT$^+$ ductal cells are regulated during homeostasis and after injury remains unknown. During development, KIT$^+$ and KRT14$^+$ cells are commonly regulated by FGF10/FGFR2b signaling (Lombaert et al., 2013; Patel et al., 2014) and the microRNA miR-133b-3p (Hayashi et al., 2017). Furthermore, manipulation of retinoic acid signaling in embryonic SMG leads to inverse expression patterns of KIT and KRT14 (Abashev et al., 2017), suggesting that these two populations may differ in response to signaling factors. Previous studies in the homeostatic and damaged ductal system have indicated that the WNT and EGF signaling pathways are active. A recent report indicates that genetic lineage tracing using the *Axin2* promoter (WNT target) traces cells in the ductal system (Weng et al., 2018), suggesting that canonical WNT signaling is, at the very least, occurring in cells capable of repopulating the ducts. In addition, expression of epiregulin and HB-EGF, factors predominantly expressed by the ducts, and their receptor EGFR have been shown to be increased in the ducts following ductal ligation injury (Nagai et al., 2014). It is also possible that KIT$^+$ and KRT14$^+$ cells are regulated by the peripheral nervous system, as we have demonstrated for cholinergic nerves and the acinar cell lineage (Emmerson et al., 2018). Further studies are needed to define the specific pathways that regulate the activity of these cells.

Our study indicates that genotoxic damage to the SG does not induce the acquisition of lineage plasticity (Fig. 8), as has been observed after injury in the intestine (Van Es et al., 2012), trachea (Tata et al., 2013) and stomach (Stange et al., 2013), where cells repopulate the lost compartment irrespective of their origin and function under unperturbed conditions. This presents a significant challenge for the tissue, as lineage plasticity of functionally distinct stem cell populations is a robust fail-safe mechanism to maintain regenerative capacity in case of stem cell loss when tissue is damaged. However, it is also possible that salivary ductal progenitor cells possess a robust response to oxidative/DNA damage and are able to efficiently repair themselves to reduce this reliance on other mechanisms. In addition, the close proximity of KIT$^+$ to KRT14$^+$ cells to each other suggests that they may behave as reciprocating niche cells, positively influencing the function of the other cell to indirectly promote repair. Further studies are required to understand their interactions and whether communication between these two cells is required for their homeostatic and regenerative capacity. In addition, whether these cells undergo plastic interconversion when under different injury conditions remains to be tested.

MATERIALS AND METHODS

Mouse lines

All procedures were approved by the UCSF Institutional Animal Care and Use Committee (IACUC) and adhered to the NIH Guide for the Care and Use of Laboratory Animals. Mouse alleles used in this study were provided

Development (2018) 145, dev166363. doi:10.1242/dev.166363

by The Jackson Laboratory and include *Krt14*^{CreERT2} (Vasioukhin et al., 1999), *Kit*^{CreERT2} (Klein et al., 2013), *Acta2*^{CreERT2} (Wendling et al., 2009), *Rosa26*^{mTmG} (Muzumdar et al., 2007) and *Rosa26*^{RFP} (Luche et al., 2007). For endogenous protein expression and proliferation analysis, C57BL/6 animals were used.

Lineage tracing of KRT14$^+$ cells

Krt14^{CreERT2};*Rosa26*^{mTmG} embryos were generated by breeding *Krt14*$^{CreERT2/+}$;*Rosa26*$^{mTmG/mTmG}$ males with *Rosa26*$^{mTmG/mTmG}$ females. Timed pregnant females were injected with 5.0 mg/20 g tamoxifen (Sigma-Aldrich) in corn oil (Sigma-Aldrich) at E10.5 and E12.5, and euthanized at E16.5, or injected with tamoxifen at E15 or E16 and euthanized at E18. For E15 and E16 embryonic analysis, n=3 and n=4 animals were analyzed, respectively. For postnatal lineage tracing of KRT14$^+$ cells, P2 or P30 pups were injected with one single dose of 0.3 mg or 5 mg tamoxifen, respectively, and euthanized at P30 (n=2) or P270 (n=1). For adult lineage tracing of KRT14$^+$ cells, 6- to 8-week-old *Krt14*$^{CreERT2/+}$;*Rosa26*$^{mTmG/mTmG}$ females were injected with one single dose of 2.5 mg/20 g tamoxifen and euthanized after 24 h (n=3) or 14 days (n=4).

Lineage tracing of KIT$^+$ cells

Postnatal lineage tracing of KIT$^+$ cells was carried out by injecting P2 *Kit*$^{CreERT2/+}$;*Rosa26*$^{mTmG/mTmG}$ pups with one single dose of 0.3 mg tamoxifen and euthanizing at P30 (n=3). For adult lineage tracing of KIT$^+$ cells, 6- to 8-week-old *Kit*$^{CreERT2/+}$;*Rosa26*$^{mTmG/mTmG}$ females and males were injected with 4 mg/30 g tamoxifen for three consecutive days and euthanized after 24 h or 14 days. For 24 h labeling efficiency, n=2 females and n=2 males were quantified. For gamma irradiation studies, *Kit*$^{CreERT2/+}$;*Rosa26*$^{mTmG/mTmG}$ adult females were injected with one single dose of 2.5 mg tamoxifen 24 h before irradiation and euthanized 30 days later (n=2).

Lineage tracing of SMA$^+$ cells

Acta2$^{CreERT2/+}$;*Rosa26*$^{RFP/RFP}$ embryos were generated by breeding *Acta2*$^{CreERT2/+}$;*Rosa26*$^{RFP/RFP}$ males with *Rosa26*$^{RFP/RFP}$ females. Timed pregnant females were injected with 5.0 mg tamoxifen at E15.5 and euthanized at E18 (n=3). For adult lineage tracing of SMA$^+$ cells, 6-week-old *Acta2*$^{CreERT2/+}$;*Rosa26*$^{RFP/RFP}$ males were injected with one single dose of 5 mg tamoxifen and euthanized 30 days (n=1) or 6 months later (n=1).

Postnatal proliferation analysis

Mouse pups were administered with 0.25 mg/25 g 5-ethynyl-2′-deoxyuridine (EdU – ThermoFisher Scientific) via subcutaneous (P2, P7 and P14) or intraperitoneal injection (P30) 2 h before collection. Submandibular glands were sectioned and processed as described.

Gamma-radiation

Gamma-radiation experiments of adult murine salivary glands were carried out as previously described (Emmerson et al., 2018). In brief, C57BL/6, *Krt14*$^{CreERT2/+}$;*Rosa26*$^{mTmG/mTmG}$ and *Kit*$^{CreERT2/+}$;*Rosa26*$^{mTmG/mTmG}$ mice were anesthetized with 1.25% 2,2,2-tribromoethanol (Alfa Aesar) in 0.9% saline (Vedco) and irradiated using a ^{137}Cs source in a Shepherd Mark-I-68A^{137}Cs Irradiator (JL Shepherd & Associates). Only the neck and part of the head were exposed, and the salivary glands were irradiated with two doses of 5 Gy at a dose rate of 167 Rads/min for 2.59 min (one of each side of the head, bilateral and sequential but on the same day) for a total dose of 10 Gy. Control mice were anesthetized as per experimental mice, but did not undergo radiation treatment. All animals were allowed to completely recover before returning to normal housing and were given soft diet *ad libitum* (ClearH_2O). Mice were euthanized after 3, 7, 14 and 30 days. For proliferation analysis, animals were injected intraperitoneally with 0.25 mg/25 g 5-ethynyl-2′-deoxyuridine (EdU – ThermoFisher Scientific) 2 h before or daily for 7 days before sacrifice.

Human salivary gland tissue collection

Human fetal salivary glands were collected from post-mortem fetuses at 22 weeks gestation with patient consent and permission from the ethical committee of the University of California San Francisco. Following dissection, salivary glands were fixed immediately in 4% PFA and fixed overnight at 4°C. Adult human salivary gland was obtained from discarded, non-identifiable tissue with consent from patients undergoing neck resection (SMG, 51-year-old male; SLG, 29-year-old male; PG, 61-year-old male). Informed consent was given by all subjects and experiments conformed to the principles set out in the WMA Declaration of Helsinki and the Department of Health and Human Services Belmont Report. Tissue was immediately transferred to ice-cold PBS to the laboratory where it was fixed in 4% PFA.

Tissue processing

Embryonic SGs were dissected and fixed for 2 h at room temperature, while adult murine, human fetal and adult human SGs were fixed overnight at 4°C, in 4% PFA. Tissue was incubated in increasing concentrations of sucrose (12.5-25%) and embedded in OCT (Tissue-Tek). Tissue was sectioned using a Leica cryostat and tissue sections kept at −20°C until immunofluorescent analysis. OCT tissue blocks were kept at −80°C.

Immunofluorescent analysis

Tissue sections were left to equilibrate at room temperature for 10 min and washed in PBS. Tissue sections were permeabilized in 0.5% Triton-X in PBS for 10 min and blocked for 2 h at room temperature in 10% donkey serum (Jackson Laboratories) and 1% BSA (Sigma-Aldrich) in 0.05% PBS-Tween-20. For anti-KIT primary antibody staining, permeabilization with ice-cold 1:1 acetone:methanol solution was carried out for 1 min, followed by incubation in blocking solution as above. Tissue was incubated overnight at 4°C in primary antibody in 0.05% PBS-Tween-20. The following primary antibodies were used: rabbit anti-SMA (1:200, Abcam, AB5694), mouse anti-SMA-Cy3 conjugated (1:400, Sigma-Aldrich, C6198), rabbit anti-AQP5 (1:200, Millipore, AB3559), rat anti-E-cadherin (1:300, Life Technologies, 13-1900), rabbit anti-KIT (1:200, Cell Signaling, 3074), goat anti-KIT (1:200, Santa Cruz, sc-1494), rabbit anti-KRT5 (1:1000, Covance, PRB-160P), rat anti-KRT8 (1:400, Troma I, DSHB), rabbit anti-KRT14 (1:1000, Covance, PRB-155P), rat anti-KRT8 (1:200, Troma II, DSHB), rat anti-KRT19 (1:300, DSHB, Troma III) and goat anti-MUC19 (1:200, AbCore, AC21-2396). For KRT14 and KIT, and KRT14 and KRT5 co-staining, rabbit anti-KRT14 (1:1000, Covance, PRB-155P) was conjugated using the Dylight 488 antibody labeling kit (ThermoFisher Scientific). Antibodies were detected using Cy2-, Cy3- or Cy5-conjugated secondary Fab fragment antibodies (Jackson Laboratories) and DNA was labeled with Hoescht 33342 (1:1000, Sigma-Aldrich). EdU staining was performed using the Click-iT EdU Alexa-Fluor 647 kit. Slides were mounted using Fluoromount-G (SouthernBiotech) and tissue was imaged using a Leica Sp5 confocal microscope and NIH ImageJ software.

Cell number and proliferation analysis

For cell number and proliferation analysis of KRT14$^+$ and KIT$^+$ cells, postnatal tissue sections and control and irradiated adult female tissue sections were stained using the Click-iT EdU kit (ThermoFisher Scientific). Cells positively stained for EdU and cell markers were counted using NIH ImageJ software. All data were obtained from a minimum of three animals for each experiment, and multiple planes throughout the SMG. Total cell counts are described in Tables S1-S10. For KRT14$^+$ SMA$^-$ cell count analysis in adult female C57BL/6 mice, intercalated-granulated duct junctions were identified and the number of KRT14$^+$ SMA$^-$ cells surrounding each duct junction was quantified and averaged over number of duct junctions counted. Total number of ducts for each time point is described in Table S7.

Statistical tests

Data were analyzed for statistical significance using a t-test (unpaired, two-tailed) or one-way analysis of variance with Tukey's multiple comparison (GraphPad Prism). For multiple testing, we used a false discovery rate of 0.05. All graphs show the mean±s.d. and were generated using GraphPad Prism.

Acknowledgements

The authors acknowledge Stacey Frumm and Dr. Aaron Tward for their assistance.

Competing interests
The authors declare no competing or financial interests.

Author contributions
Conceptualization: A.J.M., S.M.K.; Methodology: A.J.M., N.C.-P., S.M.K.; Software: S.M.K.; Validation: A.J.M., S.N., S.M.K.; Formal analysis: A.J.M., S.M.K.; Investigation: A.J.M., N.C.-P., E.E., E.A.G., S.M.K.; Resources: E.A.G., K.S., M.O.M., O.D.K., S.M.K.; Data curation: A.J.M., N.C.-P., S.M.K.; Writing - original draft: A.J.M., S.M.K.; Writing - review & editing: A.J.M., E.E., S.M.K.; Visualization: A.J.M., N.C.-P., E.E., S.N., S.M.K.; Supervision: S.M.K.; Project administration: S.M.K.; Funding acquisition: S.M.K.

Funding
The investigation was supported by grants from the National Institute of Dental and Craniofacial Research (5R01DE024188 to S.M.K.) and the National Eye Institute (5R01EY027392 and 5R01EY025980 to S.M.K.). Deposited in PMC for release after 12 months.

Supplementary information
Supplementary information available online at
http://dev.biologists.org/lookup/doi/10.1242/dev.166363.supplemental

References

Abashev, T. M., Metzler, M. A., Wright, D. M. and Sandell, L. L. (2017). Retinoic acid signaling regulates Krt5 and Krt14 independently of stem cell markers in submandibular salivary gland epithelium. *Dev. Dyn.* **246**, 135-147.

Brown, L. R., Dreizen, S., Handler, S. and Johnston, D. A. (1975). Effect of radiation-induced xerostomia on human oral microflora. *J. Dent. Res.* **54**, 740-750.

Chibly, A. M., Querin, L., Harris, Z. and Limesand, K. H. (2014). Label-retaining cells in the adult murine salivary glands possess characteristics of adult progenitor cells. *PloS One* 9, e107893.

Dreizen, S., Brown, L. R., Daly, T. E. and Drane, J. B. (1977). Prevention of xerostomia-related dental caries in irradiated cancer patients. *J. Dent. Res.* **56**, 99-104.

Dusek, M., Simmons, J., Buschang, P. H. and Al-Hashimi, I. (1996). Masticatory function in patients with xerostomia. *Gerodontology* **13**, 3-8.

El-Hashash, A. H. K. and Warburton, D. (2012). Numb expression and asymmetric versus symmetric cell division in distal embryonic lung epithelium. *J. Histochem. Cytochem.* **60**, 675-682.

Emmerson, E., May, A. J., Nathan, S., Cruz-Pacheco, N., Lizama, C. O., Maliskova, L., Zovein, A. C., Shen, Y., Muench, M. O. and Knox, S. M. (2017). SOX2 regulates acinar cell development in the salivary gland. *Elife* **6**, 433.

Emmerson, E., May, A. J., Berthoin, L., Cruz-Pacheco, N., Nathan, S., Mattingly, A. J., Chang, J. L., Ryan, W. R., Tward, A. D. and Knox, S. M. (2018). Salivary glands regenerate after radiation injury through SOX2-mediated secretory cell replacement. *EMBO Mol. Med.* **10**, e8051.

Farmer, D. T., Nathan, S., Finley, J. K., Shengyang Yu, K., Emmerson, E., Byrnes, L. E., Sneddon, J. B., Mcmanus, M. T., Tward, A. D. and Knox, S. M. (2017). Defining epithelial cell dynamics and lineage relationships in the developing lacrimal gland. *Development* **144**, 2517-2528.

Gresik, E. W. (1994). The granular convoluted tubule (GCT) cell of rodent submandibular glands. *Microsc. Res. Tech.* **27**, 1-24.

Grundmann, O., Fillinger, J. L., Victory, K. R., Burd, R. and Limesand, K. H. (2010). Restoration of radiation therapy-induced salivary gland dysfunction in mice by post therapy IGF-1 administration. *BMC Cancer* **10**, 417.

Harvey, H. (1952). Sexual dimorphism of submaxillary glands in mice in relation to reproductive maturity and sex hormones. *Physiol. Zool.* **25**, 205-222.

Hayashi, T., Lombaert, I. M. A., Hauser, B. R., Patel, V. N. and Hoffman, M. P. (2017). Exosomal MicroRNA transport from salivary mesenchyme regulates epithelial progenitor expansion during organogenesis. *Dev. Cell* **40**, 95-103.

Ito, M., Liu, Y., Yang, Z., Nguyen, J., Liang, F., Morris, R. J. and Cotsarelis, G. (2005). Stem cells in the hair follicle bulge contribute to wound repair but not to homeostasis of the epidermis. *Nat. Med.* **11**, 1351-1354.

Itzkovitz, S., Blat, I. C., Jacks, T., Clevers, H. and Van Oudenaarden, A. (2012). Optimality in the development of intestinal crypts. *Cell* **148**, 608-619.

Kim, Y.-J., Kwon, H.-J., Shinozaki, N., Hashimoto, S., Shimono, M., Cho, S.-W. and Jung, H.-S. (2008). Comparative analysis of ABCG2-expressing and label-retaining cells in mouse submandibular gland. *Cell Tissue Res.* **334**, 47-53.

Kimoto, M., Yura, Y., Kishino, M., Toyosawa, S. and Ogawa, Y. (2007). Label-retaining cells in the rat submandibular gland. *J. Histochem. Cytochem.* **56**, 15-24.

Klein, S., Seidler, B., Kettenberger, A., Sibaev, A., Rohn, M., Feil, R., Allescher, H.-D., Vanderwinden, J.-M., Hofmann, F., Schemann, M. et al. (2013). Interstitial cells of Cajal integrate excitatory and inhibitory neurotransmission with intestinal slow-wave activity. *Nat. Commun.* **4**, 1630.

Knox, S. M., Lombaert, I. M. A., Reed, X., Vitale-Cross, L., Gutkind, J. S. and Hoffman, M. P. (2010). Parasympathetic innervation maintains epithelial progenitor cells during salivary organogenesis. *Science* **329**, 1645-1647.

Knox, S. M., Lombaert, I. M. A., Haddox, C. L., Abrams, S. R., Cotrim, A., Wilson, A. J. and Hoffman, M. P. (2013). Parasympathetic stimulation improves epithelial organ regeneration. *Nat. Commun.* **4**, 1494.

Kwak, M., Alston, N. and Ghazizadeh, S. (2016). Identification of stem cells in the secretory complex of salivary glands. *J. Dent. Res.* **95**, 776-783.

Lechler, T. and Fuchs, E. (2005). Asymmetric cell divisions promote stratification and differentiation of mammalian skin. *Nature* **437**, 275-280.

Lee, M. G., Ohana, E., Park, H. W., Yang, D. and Muallem, S. (2012). Molecular mechanism of pancreatic and salivary gland fluid and HCO3 secretion. *Physiol. Rev.* **92**, 39-74.

Lombaert, I. M., Abrams, S. R., Li, L., Eswarakumar, V. P., Sethi, A. J., Witt, R. L. and Hoffman, M. P. (2013). Combined KIT and FGFR2b signaling regulates epithelial progenitor expansion during organogenesis. *Stem Cell Rep.* **1**, 604-619.

Luche, H., Weber, O., Nageswara Rao, T., Blum, C. and Fehling, H. J. (2007). Faithful activation of an extra-bright red fluorescent protein in "knock-in" Cre-reporter mice ideally suited for lineage tracing studies. *Eur. J. Immunol.* **37**, 43-53.

Man, Y. G., Ball, W. D., Marchetti, L. and Hand, A. R. (2001). Contributions of intercalated duct cells to the normal parenchyma of submandibular glands of adult rats. *Anat. Rec.* **263**, 202-214.

Marmary, Y., Adar, R., Gaska, S., Wygoda, A., Maly, A., Cohen, J., Eliashar, R., Mizrachi, L., Orfaig-Geva, C., Baum, B. J. et al. (2016). Radiation-induced loss of salivary gland function is driven by cellular senescence and prevented by IL6 modulation. *Cancer Res.* **76**, 1170-1180.

Muhvic-Urek, M., Bralic, M., Curic, S., Pezelj-Ribaric, S., Borcic, J. and Tomac, J. (2006). Imbalance between apoptosis and proliferation causes late radiation damage of salivary gland in mouse. *Physiol. Res.* **55**, 89-95.

Muzumdar, M. D., Tasic, B., Miyamichi, K., Li, L. and Luo, L. (2007). A global double-fluorescent Cre reporter mouse. *Genesis* **45**, 593-605.

Nagai, K., Arai, H., Okudera, M., Yamamura, T., Oki, H. and Komiyama, K. (2014). Epiregulin is critical for the acinar cell regeneration of the submandibular gland in a mouse duct ligation model. *J. Oral. Pathol. Med.* **43**, 378-387.

Nanduri, L. S. Y., Lombaert, I. M. A., Van Der Zwaag, M., Faber, H., Brunsting, J. F., Van Os, R. P. and Coppes, R. P. (2013). Salisphere derived c-Kit+ cell transplantation restores tissue homeostasis in irradiated salivary gland. *Radiother. Oncol.* **108**, 458-463.

Page, M. E., Lombard, P., Ng, F., Göttgens, B. and Jensen, K. B. (2013). The epidermis comprises autonomous compartments maintained by distinct stem cell populations. *Cell Stem Cell* **13**, 471-482.

Patel, V. N., Lombaert, I. M., Cowherd, S. N., Shworak, N. W., Xu, Y., Liu, J. and Hoffman, M. P. (2014). Hs3st3-modified heparan sulfate controls KIT+ progenitor expansion by regulating 3-O-sulfotransferases. *Dev. Cell* **29**, 662-673.

Redman, R. S. (2008). On approaches to the functional restoration of salivary glands damaged by radiation therapy for head and neck cancer, with a review of related aspects of salivary gland morphology and development. *Biotech. Histochem.* **83**, 103-130.

Rock, J. R., Onaitis, M. W., Rawlins, E. L., Lu, Y., Clark, C. P., Xue, Y., Randell, S. H. and Hogan, B. L. M. (2009). Basal cells as stem cells of the mouse trachea and human airway epithelium. *Proc. Natl. Acad. Sci. USA* **106**, 12771-12775.

Siegel, R. L., Miller, K. D. and Jemal, A. (2015). Cancer statistics, 2015. *CA Cancer J. Clin.* **65**, 5-29.

Srinivasan, R. and Chang, W. W. L. (1979). The postnatal development of the submandibular gland of the mouse. *Cell Tissue Res.* **198**, 363-371.

Stange, D. E., Koo, B.-K., Huch, M., Sibbel, G., Basak, O., Lyubimova, A., Kujala, P., Bartfeld, S., Koster, J., Geahlen, J. H. et al. (2013). Differentiated Troy+ chief cells act as reserve stem cells to generate all lineages of the stomach epithelium. *Cell* **155**, 357-368.

Sullivan, C. A., Haddad, R. I., Tishler, R. B., Mahadevan, A. and Krane, J. F. (2005). Chemoradiation-induced cell loss in human submandibular glands. *Laryngoscope* **115**, 958-964.

Tata, P. R., Mou, H., Pardo-Saganta, A., Zhao, R., Prabhu, M., Law, B. M., Vinarsky, V., Cho, J. L., Breton, S., Sahay, A. et al. (2013). Dedifferentiation of committed epithelial cells into stem cells in vivo. *Nature* **503**, 218-223.

Teshima, T. H. N., Ianez, R. C. F., Coutinho-Camillo, C. M., Tucker, A. S. and Lourenço, S. V. (2016). Apoptosis-associated protein expression in human salivary gland morphogenesis. *Arch. Oral Biol.* **69**, 71-81.

Tucker, A. S. (2007). Salivary gland development. *Semin. Cell Dev. Biol.* **18**, 237-244.

Van Es, J. H., Sato, T., Van de Wetering, M., Lyubimova, A., Yee Nee, A. N., Gregorieff, A., Sasaki, N., Zeinstra, L., van den Born, M., Korving, J. et al. (2012). Dll1+ secretory progenitor cells revert to stem cells upon crypt damage. *Nat. Cell Biol.* **14**, 1099-1104.

Van Keymeulen, A., Rocha, A. S., Ousset, M., Beck, B., Bouvencourt, G., Rock, J., Sharma, N., Dekoninck, S. and Blanpain, C. (2011). Distinct stem cells contribute to mammary gland development and maintenance. *Nature* **479**, 189-193.

Development (2018) 145, dev166363. doi:10.1242/dev.166363

Vasioukhin, V., Degenstein, L., Wise, B. and Fuchs, E. (1999). The magical touch: genome targeting in epidermal stem cells induced by tamoxifen application to mouse skin. *Proc. Natl. Acad. Sci. USA.* **96**, 8551-8556.

Wang, J., Zhu, H. H., Chu, M., Liu, Y., Zhang, C., Liu, G., Yang, X., Yang, R. and Gao, W.-Q. (2014). Symmetrical and asymmetrical division analysis provides evidence for a hierarchy of prostate epithelial cell lineages. *Nat. Commun.* **5**, 4758.

Wendling, O., Bornert, J.-M., Chambon, P. and Metzger, D. (2009). Efficient temporally-controlled targeted mutagenesis in smooth muscle cells of the adult mouse. *Genesis* **47**, 14-18.

Weng, P.-L., Aure, M. H., Maruyama, T. and Ovitt, C. E. (2018). Limited regeneration of adult salivary glands after severe injury involves cellular plasticity. *Cell Rep.* **24**, 1464-1470.e3.